



Pharmacological Evaluation And Characterization Of Gold Nanoparticles Targeted Treatment For Rheumatoid Arthritis

Rinkee Verma¹, Mahendra Kumar Sahu², Prafull Jain³, Rahul Singh⁴, Pramila⁴, Alka Verma⁵, Jhakeshwar Prasad^{6*}

¹Rungta College of Pharmaceutical Sciences and Research, Raipur – 492099, Chhattisgarh, India

²Kalinga University, Faculty of Pharmacy, Naya Raipur - 492001, Chhattisgarh, India

³Chhatrapati Shivaji Institute of Pharmacy, Durg – 491001, Chhattisgarh, India

⁴M. J. College, Junwani Road, Kohka – 490023, Bhilai, Chhattisgarh, India

⁵Shri Shankaracharya Institute of Pharmaceutical Science and Research, Junwani – 490020, Bhilai, Chhattisgarh, India

^{6*}Shri Shankaracharya College of Pharmaceutical Sciences, Junwani – 490020, Bhilai, Chhattisgarh, India

*Corresponding Author: Jhakeshwar Prasad

Email and Name – (Jhakeshwar Prasad)

(Received: 05 November 2023

Revised: 12 December

Accepted: 07 January)

KEYWORDS

Organic synthesis;
Rheumatoid
arthritis; Gold
nanoparticles;
Methotrexate; Drug
delivery system.

ABSTRACT:

Methotrexate (MTX) is a first-line drug for rheumatoid arthritis (RA). Targeting of MTX to inflamed joints is essential to the prevention of potential toxicity and improving therapeutic effects. Gold nanoparticles (GNPs) are characterized by controllable particle sizes and good biocompatibilities, therefore, they are promising drug delivery systems. We aimed at developing a GNPs drug delivery system incorporating MTX and folic acid (FA) with strong efficacies against RA. MTX-Cys-FA was synthesized through solid-phase organic synthesis. Then, it was coupled with sulfhydryl groups in GNPs, thereby successfully preparing a GNPs/MTX-Cys-FA nanoconjugate with targeting properties. Physical and chemical techniques were used to characterize it. Moreover, we conducted its stability, release, pharmacokinetics, biodistribution and cell cytotoxicity, cell uptake, cell migration, as well as its therapeutic effect on CIA rats. The histopathology was conducted to investigate anti-RA effects of GNPs/MTX-Cys-FA nanoconjugates. The GNPs/MTX-Cys-FA nanoconjugate exhibited a spherical appearance, had a particle size of 103.06 nm, a zeta potential of -33.68 mV, drug loading capacity of 11.04 %, and an encapsulation efficiency of 73.61%. Cytotoxicity experiments revealed that GNPs had good biocompatibilities while GNPs/MTX-Cys-FA exhibited excellent drug-delivery abilities. Cell uptake and migration experiment showed that nanoconjugates containing FA by LPS activated mouse mononuclear macrophages (RAW264.7) was significantly increased, and they exerted significant inhibitory effects on human fibroblast-like synoviocytes (HFLS) of RA ($p < 0.01$). In addition, the nanoconjugate prolonged blood circulation time of MTX in collagen-induced arthritis (CIA) rats ($p < 0.01$), enhanced MTX accumulation in inflamed joints ($p < 0.01$), enhanced their therapeutic effects ($p < 0.01$), and reduced toxicity to major organs ($p < 0.01$). GNPs/MTX-Cys-FA nanoconjugates provide effective approaches for RA targeted therapeutic strategies.

1. Introduction

Rheumatoid arthritis (RA) is a common systemic autoimmune disease that is characterized by symmetric pain and swelling of hands, wrists, feet, and knees, which impairs physical functions and quality of life. The etiology for RA has not been clearly established, however, its clinical incidence is between 0.5%- 1%. [1] The impact of RA on women is at least twice that of men. It is a disabling and painful condition that, if not

adequately treated, can lead to an immense loss of body functioning and mobility. Currently, the main chemotherapeutic options for RA treatment include glucocorticoids (GCs), nonsteroidal anti-inflammatory drugs (NSAIDs), and disease-modifying anti-RA drugs (DMARDs), including biologics and small molecule drugs. Typically, methotrexate (MTX) is the drug of choice for early RA treatment. It can effectively treat RA at low doses (15–25 mg/week). [2] Clinically,



MTX is associated with adverse reactions, including bone marrow suppression, gastrointestinal discomfort, mucosal skin damage, and neurotoxicity. Therefore, regular monitoring during administration is required. Furthermore, 80% of MTX is metabolized in the kidneys, leading to nephrotoxicity, severe neutropenia, sepsis, and finally, advanced renal failure. Currently, targeting drugs to joints is a new trend in RA treatment. To achieve effective drug delivery, nanomedicine has become an effective strategy for RA treatment. Various types of nanocarriers, including liposomes polymer micelles dendrimers and gold nanoparticles (GNPs) among others, are widely used for the delivery of anti-RA drugs through active or passive targeted systemic administration. The GNPs are excellent drug carriers for RA treatment. GNPs are essentially nontoxic, stable, and reliable *in vivo*, and have unique optical properties, adjustable sizes and shapes, easy surface modification, good biocompatibility, and easy binding to active ligands through Au-S chemical bonds. [3] The therapeutic potential of GNPs can improve treatment outcomes for current RA treatments by linking various ligands to stimulate immune system protection, targeting, cell internalization, and delivery of therapeutic payloads. Given that nanoparticles efficiently accumulate in inflammatory microenvironments of arthritic joints, development of nano-drugs for RA has rapidly increased. These microenvironments are characterized by angiogenic vessels and abnormal peripheral lymphatic systems. Abnormal proliferations of synovial cells that normally form a lining in synovial joints induce anoxic and nutrient-deficient microenvironments and massive angiogenesis. Correspondingly, under the stimulus of an inflammatory environment, due to mutual pulling of the vascular endothelium, a gap of about 700 nm is formed between the vascular endothelium. The spleen can remove nanoparticles larger than 200 nm, and the threshold of renal clearance is about 10 nm. [4] Therefore, 10 nm-200 nm nanoparticles can penetrate endothelial tissues to treat RA through passive targeting. A large number of activated macrophages in RA synovial joints are an important cause of joint inflammation. Activated macrophages and fibroblast-like synoviocytes (HFLS) attach to bone and cartilage junctions, forming a destructive pannus. Moreover, activated macrophages overexpress a large number of pro-inflammatory factors, including tumor necrosis factor alpha (TNF- α), interleukin-1 β (IL-1 β), and interleukin-6 (IL-6) among others, which trigger synovial membrane inflammation and synovial hyperplasia. Cartilage loss and bone damage play a role in promoting RA progression. Activated macrophages also express many receptors, such as folate receptor (FR) and scavenger receptor (SR). Accumulation of activated macrophages in arthritis sites allows folic

acid (FA) and therapeutic drugs to selectively target these inflammatory sites. [5] In this manner, FA targeted therapies can selectively attack inflammatory cells without harming healthy macrophages. Therefore, activated macrophages are a potential target for active targeted RA therapy. FR is a glycerol phosphoinositide-linked membrane glycoprotein. Three FR isoforms, which are, α -FR, β -FR and γ -FR have been identified. The FA-drug copolymer binds FR on the surface of macrophages and is enriched in a specific area of target cells (the inclusion body is covered with a small recess), which sinks into the cytoplasm to form an endocytic cavity, called an early endosome. Due to the ion pump action, the pH value of the endocytic cavity drops to 5 after which a large amount of carboxyl matrix in the FR protein is protonated and the configuration changes. Then, the drug and FA are broken after which the drug crosses the endosomal capsule and enters the macrophage nucleus to exert its activity. [6] FA molecules can be excreted from cells by reducing the folate carrier. Since the FA-drug conjugate cannot escape the cell membrane through the folate carrier, this mechanism ensures that anti-RA drugs can effectively act on the nucleus, while suppressing toxic side effects on normal cells. In addition, RA patients often suffer from FA deficiency, while FA reserves of RA patients receiving MTX treatment are further reduced. Suppressed intracellular folate levels have been reported in liver cells and in peripheral blood lymphocytes of MTX administered patients. Most of the studies on gastrointestinal and hematological side effects are related to FA deficiency. Therefore, FA supplementation may reduce the side effects associated with MTX treatment. [7] In this study, we designed a novel nanoparticle drug carrier system. A spherical GNPs loaded MTX was synthesized through a series of three steps, including: i. Synthesis of GNPs through the sodium citrate reduction method; ii. Synthesis of MTX-Cys-FA by solid-phase organic synthesis method, and iii. Conjugation of GNPs with MTX-Cys-FA to obtain novel nanoscale targeted drug carrier systems. Then, we investigated: i. The physicochemical properties of the synthesized GNPs and GNPs/MTX-Cys-FA; ii. The effects of the nanoconjugate on cell toxicity and LPS uptake by activated and inactivated RAW264.7 cells; iii. The effects of nanoconjugates on horizontal and vertical migration of HFLS-RA cells and iv. *In vivo* pharmacokinetics, bio-distribution, therapeutic effects, and safety properties of free MTX and GNPs/MTX-Cys-FA. Our findings show the potential significance of synthetic GNPs/MTX-Cys-FA in the treatment of RA. [8]

2. Materials and methods

2.1. Materials



Tetrachloroauric acid and methotrexate were obtained from Sigma-Aldrich, Mumbai (Maharashtra, India). Folic acid was purchased from Sigma-Aldrich, Mumbai (Maharashtra, India). The resins, Fmoc-Lys-(DDE)-OH and Fmoc-Cys (Trt)-OH were purchased from Sigma-Aldrich, Mumbai (Maharashtra, India). S-Trityl-L Cysteine (Cys) was purchased from Sigma-Aldrich, Mumbai (Maharashtra, India). TNF- α was purchased from Loba Chemie Pvt. Ltd. Mumbai (Maharashtra, India). The DMEM medium and fetal bovine serum were sourced from Loba Chemie Pvt. Ltd. Mumbai (Maharashtra, India). Penicillin and streptomycin were purchased from Loba Chemie Pvt. Ltd. Mumbai (Maharashtra, India). The lipopolysaccharide (LPS) was obtained from Sigma-Aldrich, Mumbai (Maharashtra, India). 4', 6 diamino-2-phenylindole dihydrochlorides (DAPI) and fluorescein isothiocyanate (FITC) were purchased from Sigma-Aldrich, Mumbai (Maharashtra, India). Bovine type II collagen and Freund's incomplete adjuvant were obtained from Sigma-Aldrich, Mumbai (Maharashtra, India). The ELISA kit was purchased from Sigma-Aldrich, Mumbai (Maharashtra, India).

2.2. Solid-phase organic synthesis of MTX-Cys-FA

To synthesize the solid phase organic MTX-Cys-FA, 1 g of the MBHA resin was put in a reaction tube. Then DMF was used to dissolve the resin, Fmoc-Cys (Trt)-OH (0.3 mmol) and DIC (1.5 mL) were added to the solution and shaken for 60 min. The resin was washed 3 times using DMF, DCM, DMF and blocked with acetic anhydride. After the reaction, the solution was drained out from the reaction tube, then, 20% piperidine in DMF solution was added to react for 15 min. Fmoc-Lys (DDe)-OH (0.9 mmol) was added and concentrated with DIC for 60 min. The resin was drained and 20% of the piperidine DMF solution added for 5 min to remove the deprotection agent. Then 3 times the amount (0.9 mmol) of FA was added and concentrated with DIC (1–2 mL) for 30 min. The resin was sequentially washed using DMF, DCM, and DMF, eluted twice (3–5 min each time) using 2% hydrazine hydrate/DMF solution after which three times the amount (0.9 mmol) of MTX was added, concentrated using DIC (1–2 mL) for 30 min, washed and drained to prepare the lysate: TFA 95%; water 1%; EDT 2%. The peptide was cleaved from the resin. The cleavage time was 120 min. The lysate was blown dry using nitrogen, washed 6 times using ether, and evaporated to dryness at room temperature. Schematic presentation of the synthesis process is shown in fig.1. The crude product was purified by high-performance liquid chromatography and lyophilized to collect the target peptide solution, then placed in a freeze dryer (Advantage 2.0, SP Scientific, Warminster, PA, USA) precooled at - 80 °C for 0.5 h, sealed immediately after

vacuum drying for 48 h, and stored at - 4 °C for detection. The HPLC system included a CBM-20 pump, a SIL-20 autosampler, a CTO-20A column oven, and an SPD-20A UV/Visible detector set at 220 nm. Samples were analyzed on the Gemini-NX C18 column (4.6 \times 250 mm) under the following conditions. Mobile phase A: 0.1% trifluoroacetic in 100% acetonitrile, mobile phase B: 0.1% trifluoroacetic in 100% water vacuum degassing, 0.01 min: (18%: 82%); 25 min: (53%: 47%); 25.01 min: (100%: 0%); 30 min: stop. The sample was filtered through a 0.22 μ m microporous membrane before use. The flow rate was 1.0 mL/min, chromatographic conditions were 35 °C while the injection volume was 10 μ L. The retention time of the purified sample was 11.24 min.

2.3. Preparation of GNPs and GNPs/MTX-Cys-FA

In this study, GNPs were synthesized by reduction of HAuCl₄ solution with sodium citrate solution. [9] Accurately weighed 0.1 g sodium citrate was added into 10 mL deionized water. A 100 mL aqueous solution of 0.01% (w/v) HAuCl₄ was placed into a three necked round-bottom flask, in an oil bath (140 °C), and a rotation speed of 10 rpm. After the solution is heated to boiling, quickly add 2 mL of 1% sodium citrate solution to the three-necked flask, and the color of the solution becomes stable red after 2 min. The solution was boiled for 15 min, then cooled to room temperature under stirring for 2 h. In this experiment, the principle that gold and sulfhydryl can form a coordination bond, to make the sulfhydryl-containing compound self-assemble on its surface to obtain stable nanoparticles was used. Briefly, 1 mg of the freeze-dried powder of MTX-Cys-FA was slowly added to 10 mL of the GNPs solution and stirred overnight at room temperature under dark conditions. The resulting solution was centrifuged, the supernatant was discarded, ultrapure water was added, washed 3 times by ultrasonic vibration to remove unreacted components, and freeze-dried to obtain the GNPs/MTX-Cys-FA powder.

2.4. In vitro characterization of GNPs and GNPs/MTX-Cys-FA

About 4 mL of the prepared GNPs solution and GNPs/MTX-Cys-FA solution at a pH of 7.4 were used to measure the particle sizes, polydispersity indices (PDI), and zeta potentials using a high-sensitivity zeta potential and particle size analyzer. Drops of the prepared GNPs solution and GNPs/MTX-Cys-FA solution on a copper sheet were observed by transmission electron microscopy. Take the freeze-dried GNPs/MTXCys-FA powder and place it on the copper sheet after which their morphological characteristics were observed using a scanning electron microscope images were obtained. The chemical



structure of the nanoconjugate was determined using a fourier transform infrared (FTIR) spectrophotometer. The X-ray diffraction (XRD) spectrometer was used to perform XRD scanning on freeze-dried powders of MTX, FA, and MTX-Cys-FA to observe crystal structure changes. The scanning range 2θ was $5-40^\circ$. Differential scanning calorimetry (DSC) and thermogravimetric analyses (TGA) were performed to evaluate thermal stabilities of GNPs and thermal

changes during heating. A differential scanning calorimeter was used for DSC studies of MTX, FA and GNPs/MTX-Cys-FA. The DSC thermogram was used to provide information on physical properties of the sample. The sample was scanned between $0^\circ\text{C}-300^\circ\text{C}$ at a rate of $10^\circ\text{C}/\text{min}$. TGA was carried out on a Linseis 1600 analyzer. Analyses were performed at a heating rate of $10^\circ\text{C}/\text{min}$, temperature range of $35^\circ\text{C}-750^\circ\text{C}$ and at an airflow rate of $4\text{ mL}/\text{min}$.

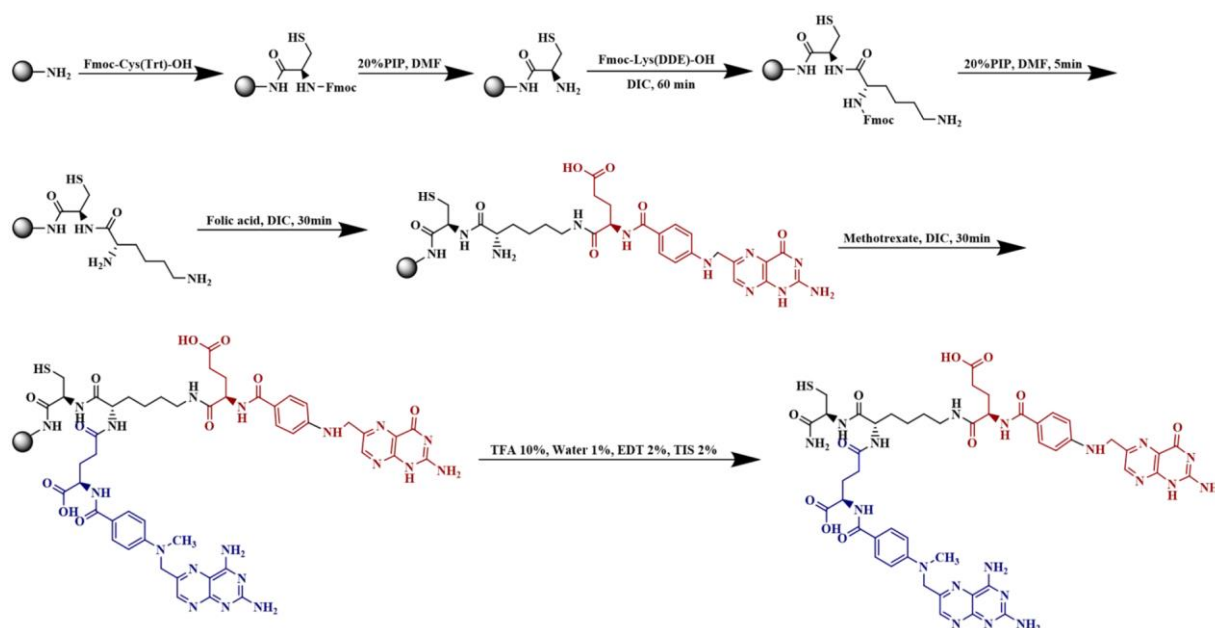


Fig.1. Chemical reaction flow for solid phase organic synthesis of MTX-Cys-FA.

2.5. Evaluation of the stability of GNPs and GNPs/MTX-Cys-FA

Freeze-dried powders of GNPs and GNPs/MTX-Cys-FA were suspended in different solutions (deionized water, PBS at pH 7.4, and PBS with 10% fetal bovine serum). Then, they were incubated at 4°C and 37°C for 7 days. Particle size changes of GNPs and GNPs/MTX-Cys-FA were simultaneously measured to evaluate their stability.

2.6. Hemolysis test

Blood compatibilities of GNPs/Cys-MTX-FA and free MTX were evaluated by spectrophotometry. Briefly, 15 mL of fresh rabbit blood was centrifuged at 4000 rpm for 15 min to separate red blood cells. After repeated washing, different concentrations of GNPs/MTX-Cys-FA and free MTX were added to 2% (*v/v*) RBC. After mixing, incubation was done at 37°C for 4 h. Normal saline (NS) was used as the negative control while 1% heparinized normal saline was used as the positive control. After taking pictures, samples were centrifuged at 4000 rpm for 10 min. Approximately 100 μL of

supernatants for each sample were used to measure absorbance of free hemoglobin using a microplate reader at a wavelength of 540 nm. The hemolysis rate was determined using the following formula.

$$\text{Hemolytic ratio (\%)} = \frac{A_{\text{sample}} - A_{\text{negative control}}}{A_{\text{positive control}} - A_{\text{negative control}}} \times 100\%$$

Where, A_{sample} , $A_{\text{negative control}}$, and $A_{\text{positive control}}$ represent the absorbances of the sample, and negative as well as positive controls, respectively.

2.7. In vitro release of drugs

To evaluate the release of GNPs/MTX-Cys-FA in a neutral physiological environment (pH 7.4) and in an acidic intracellular environment (pH 5.5), PBS at different pH levels was selected as the *in vitro* release medium. The freeze-dried nanoparticles (1 mg) were resuspended in 1 mL PBS (pH 7.4 or pH 5.5), put in a 3500 Da dialysis bag, which was transferred to 40 mL PBS (pH 7.4 or pH 5.5) and incubated at 37°C with constant stirring at 120 rpm. Sampling was performed at predetermined times (0.5 h, 1 h, 2 h, 4 h, 6 h, 8 h, 10 h, 12 h, 24 h). At each sampling time, 1 mL of the



sample was obtained. The *in vitro* release fluid was replaced with an equal volume of fresh PBS buffer at the corresponding pH value. Drug concentrations in the *in vitro* release solution were determined in triplicates by HPLC in the supplementary material. Cumulative drug releases (F) were calculated according to the formula. Then, the drug release curve was drawn

$$F = C_n V + \sum_{i=n-1}^1 C_i V_i$$

$$M_{\text{Drug}} \times 100\%$$

Where F : cumulative drug release rate; C_n : drug osmotic concentration at the sampling time point; V : total volume of dialysate; C_i : drug concentration at the previous sampling point; V_i : sampling volume; M_{drug} : total drug volume in the dialysis bag.

2.8. Drug loading experiment

Drug loading and encapsulation efficiencies of the nanoconjugates were determined by HPLC. Briefly, the GNPs/MTX-Cys-FA (13,000 r, 15 min) were centrifuged and the supernatant collected. Ultrapure water was added to the precipitate and sonicated for 10 min. These processes were repeated thrice, after which the supernatants were combined. Formulas for calculating DL% and EE% were as follows:

$$DL (\%) = \frac{M_{\text{total}} - M_{\text{supernatant}}}{M_{\text{nanoparticles}}} \times 100\%$$

$$EE (\%) = \frac{M_{\text{total}} - M_{\text{supernatant}}}{M_{\text{total}}} \times 100\%$$

In the formula, M_{total} represents the total mass of MTX; $M_{\text{supernatant}}$ represents the total mass of supernatant MTX; $M_{\text{nanoparticles}}$ represents the total mass of nanoparticles.

2.9. CCK-8 assay for cytotoxicity of GNPs to RAW264.7

To evaluate the cytotoxicity of blank GNPs to RAW264.7 cells, activated (cultured in LPS medium containing 1000 ng/mL for 48 h) or inactivated RAW264.7 cells were seeded in 96-well plates (2.0×10^4 cells/well). They were incubated for 24 h after which the culture medium was obtained. Then, different concentrations of GNPs solutions (50 $\mu\text{g/mL}$, 25 $\mu\text{g/mL}$, 10 $\mu\text{g/mL}$, 1 $\mu\text{g/mL}$, and 0.1 $\mu\text{g/mL}$) were added in the culture medium. The blank control was the medium without the GNPs solution. After 24 h or 48 h, the supernatant was discarded and 100 μL of DMEM medium containing 10% CCK-8 reagent added to each well. Incubation was done at 37 $^\circ\text{C}$ for 1.5 h, then, spectrometric absorbance at 540 nm was measured using a microplate reader.

2.10. FITC labeling GNPs/MTX-Cys-FA

Fluorescein isothiocyanate (FITC) yellow powder (2 mg) was dissolved in 1 mL ethanol. Under continuous stirring, the solution was added dropwise to MTX-Cys-FA or MTX-Cys suspension, and reacted at room temperature away from light for 24 h. The obtained

solution was dialyzed using double distilled water (molecular weight between 12 and 14 kDa) to remove free FITC, and lyophilized to obtain FITC-labeled nanoparticles. Synthesis of GNPs/MTX-Cys-FA-FITC and GNPs/MTXCys-FITC were done as described in Section 2.3.

2.11. Cytotoxicity of free MTX and nanoparticles

To evaluate the cytotoxicity of free MTX and nanoparticles, HFLS-RA cells were seeded in a 96-well plate and incubated for 24 h. Then, different concentrations of GNPs, GNPs/MTX-Cys-FA or free MTX solutions (50 $\mu\text{g/mL}$, 25 $\mu\text{g/mL}$, 10 $\mu\text{g/mL}$, 1 $\mu\text{g/mL}$, 0.1 $\mu\text{g/mL}$) were diluted in the culture medium. The blank control was the medium without added drugs. After 24 h or 48 h, the supernatant was discarded. About 100 μL of the DMEM medium with 10% CCK-8 reagent was added to each well and incubated at 37 $^\circ\text{C}$ for 1.5 h, then, spectrometric absorbance at 540 nm was measured using a microplate reader.

2.12. HFLS-RA cell proliferation assay

HFLS-RA cells pretreated with free MTX or GNPs/MTX-Cys-FA with or without TNF- α (100 ng/mL) for 24 h were seeded into 96-well plates (5×10^3 pcs/well). GNPs/MTX-Cys-FA, with MTX concentrations of 5 $\mu\text{g/mL}$, 2.5 $\mu\text{g/mL}$, and 1.25 $\mu\text{g/mL}$, were added to the culture medium. The blank control was composed of cells without treatment while to the negative control group, TNF- α was added while no drugs were added.

Incubation was done for 24 h after which the supernatant was discarded. The DMEM medium (100 μL) containing 10% CCK-8 reagent was added to each well. The spectrometric absorbance at 540 nm was measured using a microplate reader.

2.13. HFLS-RA cell assay for horizontal migration

Effects of free MTX or GNPs/MTX-Cys-FA on horizontal migration of HFLS-RA cells were determined via the wound healing assay. HFLS-RA cells were seeded into 6-well plates (1×10^5 pcs/well) and incubated for 24 h. Upon reaching 90% confluence, cells were cultured in blank DMEM for 12 h. A 20 μL pipette tip was used to scratch the cell surface. Cells were gently washed thrice using PBS to remove floating cells. Negative control cells were treated with TNF- α (100 ng/mL) only while experimental cells were treated with different concentrations of MTX and GNPs/MTX-Cys-FA drug solutions (5 $\mu\text{g/mL}$, 2.5 $\mu\text{g/mL}$, and 1.25 $\mu\text{g/mL}$). Incubation was performed at 37 $^\circ\text{C}$ in a 5% CO₂ environment for 0 h, 6 h, 12 h, and 24 h. Cells were observed under a 100x inverted microscope,



photographed and the ImageJ software v1.6.0 was applied to measure the distance of cell migration.

2.14. Transwell assay for HFLS-RA cell migration

Effects of free MTX or GNPs/MTX-Cys-FA on vertical migration of HFLS-RA were detected through transwell assays. About 600 μL of drug solutions (5 $\mu\text{g}/\text{mL}$, 2.5 $\mu\text{g}/\text{mL}$, and 1.25 $\mu\text{g}/\text{mL}$) with or without TNF- α (100 ng/mL) were added in the lower chamber (8 μm) of the transwells. In the upper chamber of the transwell, HFLS-RA (1×10^5 pcs/well) were seeded after which 100 μL of the medium containing different concentrations of the drug were added. Incubation was performed for 14 h. Cells were removed from the transwells chamber. A cotton swab was used to remove cells that had not invaded the surface of the transwells chamber, gently rinsed using PBS, dried, and fixed in 4% paraformaldehyde. After 30 min, cells were stained with 0.1% crystal violet for 1 h. Excess crystal violet was removed by rinsing using double distilled water and dried. Cell invasions were evaluated under a 100x inverted microscope and photographed.

2.15. Therapeutic efficacy evaluations in vivo

To induce CIA, Wistar rats were subcutaneously injected with bovine type II collagen (2 mg/mL) and incomplete Freund's adjuvant (CFA, 2 mg/mL). About 200 μL of the emulsion was injected at 3 cm under the skin of rat tails as initial immunizations. After 7 days, rats were again immunized with 100 μL emulsion at the same concentration. The success of model establishment was evaluated using inflammatory scores of rat joints. To investigate the therapeutic effects of GNPs/MTX-Cys-FA on the established Wistar rat models, the CIA rat models were randomly allocated into 5 groups ($n = 5$). On the 21st day after establishing the rat models, rats in the blank group were administered with normal saline, rats in the positive control group were administered with MTX injection

(1.5 mg/kg). GNPs/MTX-Cys-FA was administered injection at high, medium and low doses (3 mg/kg , 1.5 mg/kg and 0.75 mg/kg , respectively). Administrations were done every other day for a total of 5 times (23–31 days). Toe volumes for every CIA rat model were recorded at the time of administration. To investigate the potential adverse effects of nanoconjugates on CIA rat models, body weights of rats in each group were determined on the 23rd to 33rd days. The timeline for animal experiments was as shown in Fig. 2.

2.16. Micro-CT imaging

After treatment of rat models, three-dimensional reconstruction images of ankles and hind paws were developed by Micro-CT. Rat models were anesthetized using ether. Then, their left hind paws were obtained and fixed in 4% paraformaldehyde for 24 h. Samples were scanned by Micro-CT to obtain the constructed three-dimensional images.

2.17. Histopathology analysis

To investigate the pathological changes associated with rat arthritis, HE staining was performed. Briefly, rat ankle right joints were fixed in 4% paraformaldehyde for 2 days after which 10% EDTA was used for decalcification for 30 days. Finally, they were embedded in paraffin, sectioned and imaged. A microscope was used to observe tissue sections and to analyze arthritis severity, and a 10x objective for analysis of the histological synovitis score (HSS) to measure synovitis status and modified osteoarthritis research society international (OARSI) scores to assess articular cartilage status. [10]

2.18. Enzyme-linked immunosorbent assay

After treatments, serum was obtained from CIA rat models and levels of IL-6, IL-17, IL-1 β , TNF- α as well as TRAP levels detected using an ELISA kit according to the manufacturer's instructions.

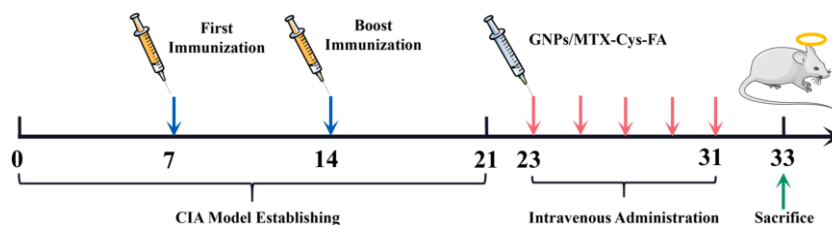


Fig. 2. Time axis of animal experimental progress.

2.19. Statistical analysis

Data are expressed as mean \pm standard deviation (SD). Statistical analyses were performed using the SPSS software. Statistical significance was analyzed using Student's t-test significance. $P \leq 0.05$ was considered to be statistically significant, while $p \leq 0.01$ and $p \leq 0.001$ were considered to be very significant.

3. Results and discussion

3.1. Characterizations of the synthesized conjugates and GNPs

Particle sizes and zeta potentials of GNPs as well as nanoconjugates in the pH 7.4 aqueous solution were measured through the DLS technology (Table 1).



Particle sizes of the GNPs were determined to be 22.83 ± 0.29 nm. After drug loading, particle sizes of the nanoparticles increased significantly (103.06 ± 3.88 nm). Because of their enhanced penetration and retention (EPR) effects, nanoparticles have been shown to be suitable for passive targeted drug aggregation at the diseased site and are also suitable for intravenous administration for RA treatment. [11] Zeta potential is a key factor that affects the stability of suspended nanosphere colloids. When dispersed in deionized water, the zeta potential of GNPs was found to be -68.02 ± 2.59 mV. After incorporation of the GNPs, surface potentials of nanoparticles changed significantly, reaching -33.68 ± 1.02 mV. Moreover, the addition of MTX-Cys-FA led to a significant increase in surface charge, indicating that charges of the nanoparticles had changed, which weakened the negative effect. MTX-Cys-FA resulted in the formation of a dense shell on the nanosphere surface. Changes in surface charges alters dielectric states of nanoparticles, thereby reducing their electrophoretic mobilities and ultimately, resulting in a decrease in zeta potentials. [12] We found that GNPs/MTX-Cys-FA was still in a relatively stable state when it reached the maximum drug load. The GNPs maintain the maximum drug load, so that they can be used as carriers to achieve the best drug delivery capacity in the body and reduce their accumulation in the body. According to SEM and TEM analyses, GNPs structures were identified as monodisperse regular spherical shapes, consistent with PDI results obtained by DLS (Fig. 1D and F). TEM analysis of GNPs/MTX-Cys-FA revealed that it was spherical and that the surroundings were adsorbed. When observed in SEM, surfaces of nanoparticles appeared blurred due to the large charge effect after drug coupling. These findings indicate that nanoconjugates have a high zeta potential (close to 30 mV) and good stability (Fig. 1E and G). Spherical nanocarriers have a higher specific surface area than other morphological structures, therefore, they exhibit better anti-inflammatory drug binding abilities. The FTIR technology was used to investigate the chemical structure of the nanoconjugate and to verify the synthesis of GNPs/MTX-Cys-FA synthesis. The FTIR spectrum of the synthesized product was as shown in Fig. 2A and B. Infrared spectrum of cysteine revealed that 2633 cm^{-1} is the absorption band of the sulfhydryl group (the stretching vibration of the SH group), 3499

cm^{-1} is the absorption band of the specific group of the amine group (the NH group stretching vibration), and 1698 cm^{-1} is the absorption band of the specific group of the carboxyl group (the stretching vibration of the C = O group). Absorption bands of 1602 cm^{-1} (the stretching vibration of aromatic ring C = C and C = N) and 3316 cm^{-1} (the N–H stretching vibration of the amine group) are used as specific absorption bands for FA. among them, the absorption bands at 1676 cm^{-1} in FA and 1673 cm^{-1} of MTX are assigned to the absorption band of the carboxyl group (the stretching vibration of C = O group). The most significant change in MTX-Cys-FA is that, at 1700 cm^{-1} , there was no absorption band belonging to the carboxyl group. In addition, the absorption peak at 1237 cm^{-1} is band I absorption peak of the amide bond, the absorption peak at 1540 cm^{-1} is band II absorption peak of the amide bond, while the absorption peak at 1338 cm^{-1} is band III amide bond. These findings confirm that an amide reaction occurred between MTX, Cys, and MTX to form an amide bond. MTX-Cys-FA reacts with GNPs through the sulfhydryl group of Cys. Fig. 2B shows that the FTIR of GNPs/MTX-Cys-FA did not have a sulfhydryl peak, proving that Cys chemically bound to surfaces of GNPs, confirming that MTX-Cys-FA was bound to the surface of GNPs through sulfhydryl groups. After more than 50 years of continuous development, solid-phase organic synthesis has greatly promoted the development of peptides as therapeutic drugs, including the construction of amide/peptide bonds involving the combination of carboxylic acids, amines, and other additives. [13] Both MTX and FA have carboxyl and amino groups, therefore, they exhibit similar properties to amino acids. The linker is a bifunctional molecule. It allows anchorage to the carrier and at the same time, it exhibits the characteristics of a protective group. Cys is the most common amino acid with a sulfhydryl group. Therefore, Cys is usually used as a linker to perform the solid-phase organic synthesis of MTX and FA. It has various advantages. Its biggest advantage is that all purification steps during synthesis are completed by simple washing and filtering, greatly reducing the difficulty in purification. It also has the advantages of convenience and quickness, simple operation, and high yield. Moreover, its superiority is expressed by the ease of its automation, therefore, it has become the preferred method for peptide chemical synthesis.

Table 1. Physicochemical property of GNPs and GNPs/MTX-Cys-FA ($n = 3$).

Nanoparticles	Size (nm)	PDI	Zeta potential (mV)	EE (%) MTX	DL (%) MTX
GNPs	22.83 ± 0.29	0.08 ± 0.04	-68.02 ± 2.59		
GNPs/MTX-Cys-FA	103.06 ± 3.88	0.29 ± 0.22	-33.68 ± 1.02	73.61 ± 1.91	11.04 ± 0.28

Abbreviations: PDI, polydispersity index; EE, encapsulation efficiency; DL, drug loading.

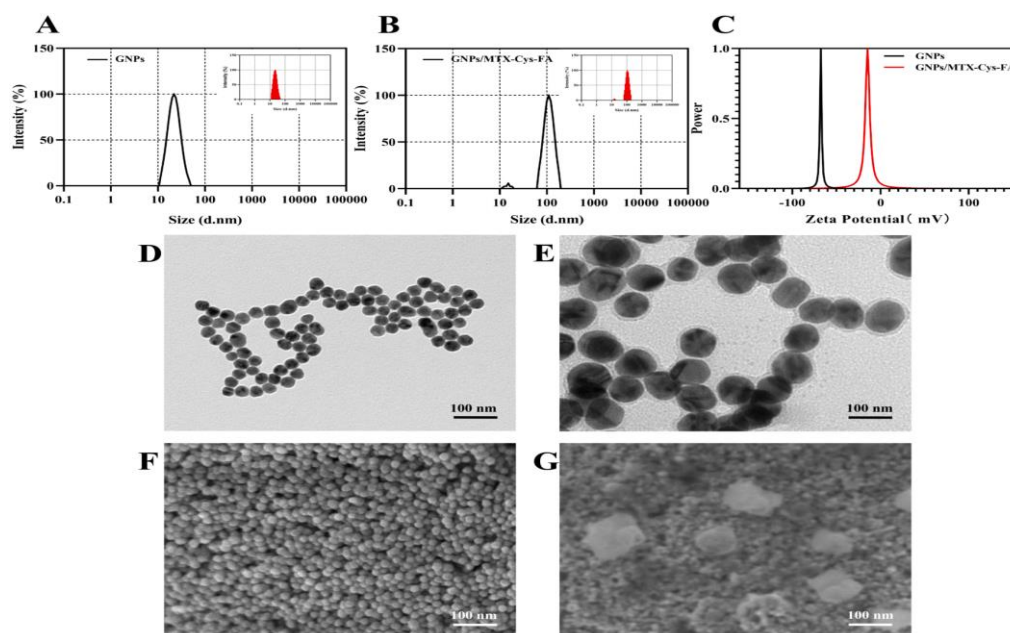


Fig. 3. Particle size, zeta potential and morphological observation. (A) Particle size of GNPs. (B) Particle size of GNPs/MTX-Cys-FA. (C) Zeta potential of GNPs and GNPs/MTX-Cys-FA. (D) TEM images of GNPs. (E) TEM images of GNPs/MTX-Cys-FA. (F) SEM images of GNPs. (G) SEM images of GNPs/MTX-Cys-FA. Scale 100 nm.

Analysis of X-ray diffraction spectra of MTX, FA, and GNPs/MTX-Cys-FA were also performed. Fig. 2C shows that FA and MTX exhibited strong crystal absorption peaks at multiple diffraction angles. FA and MTX were found to exhibit sharp peaks from 10° to 40° confirming its crystalline nature while decrease in intensity of the crystalline peaks in GNPs/MTX-Cys-FA confirmed the absorption of MTX-Cys-FA on the surface of GNPs as shown in Fig. 2C. [14] DSC was used to evaluate the crystallinity of compounds and their possible interactions. Fig. 2D shows the heat maps of MTX, FA, and GNPs/MTX-Cys-FA. The DSC curve of MTX exhibited an endothermic peak at 116°C . In the thermogram of FA, there was an endothermic peak at 128°C . However, the DSC curve obtained from GNPs/MTX-Cys-FA did not show MTX and FA melting peak. The absence of phase transitions owing to MTX and FA in the DSC analysis is evidence that they are noncrystalline state on the surface of GNPs. This also confirms the results obtained from the XRD study. [15] TGA was performed to determine the proportion of organic compounds. Fig. 2E shows that exothermic decomposition of GNPs/MTX-Cys-FA occurred in the $110\text{--}700^\circ\text{C}$ range, while total weight loss was 64%. Comparatively, the overall Au content accounted for 36%, while drug loading capacity of GNPs/MTX-Cys-FA was 12.2%.

3.2. Stability and hemolysis tests

Nanoparticle stability is very important for their preservation. Table 2, Fig. 3A and C show that at 4°C , GNPs in any medium did not change significantly from

day 0 to day 7. From day 5 to day 7, particle sizes of GNPs/MTX-Cys-FA in PBS supplemented with 10% FBS increased significantly, the value of zeta potential becomes slightly smaller, indicating nanoparticle aggregation. These data support the storage of GNPs and GNPs/MTX-Cys-FA without serum at 4°C . Fig. 3B and D show the stability of GNPs and GNPs/MTX-Cys-FA in different media at 37°C . Particles sizes of GNPs and GNPs/MTX-Cys-FA in all experimental media were not unchanged within 3 days. From the 4th day to the 7th day, particle sizes of GNPs increased slowly, and the value of zeta potential becomes smaller. This may be attributed to collisions of spherical GNPs at 37°C , which caused colloidal solutions to coagulate. From day 4 to day 7, particle sizes of GNPs/MTX-Cys-FA increased sharply in PBS supplemented with 10% FBS, and the value of zeta potential decreased rapidly. The results showed that GNPs/MTX-Cys-FA remained stable for at least 3 days when simulating the *in vivo* environment, and could exist stably for at least 7 days under a storage environment of 4°C . It is proved that GNPs/MTX-Cys-FA nanoparticles can quickly reach complete distribution in the body after intravenous injection. Many studies have similar results, Sun et al. (2019) used PK3 and FA-PEG-PLGA as carriers to encapsulate siRNA to prepare acid-sensitive polymer nanoparticles (FA-siRNA-PPNPs). At 37°C , it could only exist stably for 2 days, and obvious aggregation appeared on the third day, but the *in vivo* delivery of nanoparticles was not affected. In addition, according to pharmacokinetic experiment results 3.6, the half-life



of GNPs/MTX-Cys-FA *in vivo* was 3.202 ± 0.26 h, and the average residence time was 3.82 ± 0.215 h, indicating that the residence time of GNPs/MTX-Cys-

FA *in vivo* was not more than 3 days, and the drug could be fully released in rats to achieve efficacy.

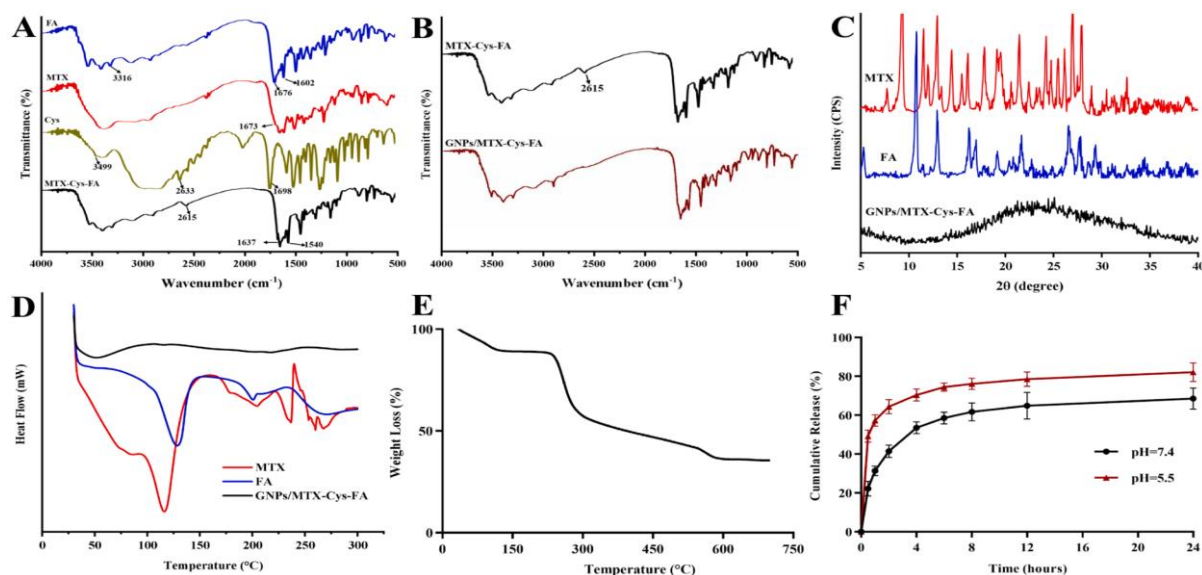


Fig. 4. Physical and chemical characterization diagram. (A and B) FTIR characterization of synthetic nanoparticles. (C) X-ray diffraction (XRD) spectra and differential scanning calorimetry (DSC) thermograms (D) of MTX, FA and GNPs/MTX-Cys-FA. (E) TGA graph of GNPs/MTX-Cys-FA. (F) The *in vitro* release behavior of GNPs/MTX-Cys-FA under different pH (7.4 and 5.5) environments.

These findings demonstrate that GNPs and GNPs/MTX-Cys-FA exhibit good stability after storage and administration, suggesting that the nanoconjugates can be safely and stably delivered to patients within 3 days. Although the delivery mechanism of nanoparticles *in vivo* is not clear, such as drug absorption and release rates. However, some pharmacokinetics and *in vivo* drug distribution experiments have theoretically increased the research progress of its delivery rules. [16] These research advances provide the possibility for the stable delivery of nanoconjugates. During the period from the manufacture of the GNPs/MTX-Cys-FA nanoconjugate to the delivery of the patient, it can be made into a powder injection for storage and transportation during the period from manufacturing to patient delivery. For example, Ma et al. (1999) used cyclodextrin derivatives (SBE) 7 α - β -CD and HP- β -CD as alternative delivery vehicles for injectable melphalan formulations, which are very stable within 1 year after lyophilization. Refer to the FDA instructions for MTX, the adult dosage is 7.5- 15 mg/week, and we chose a dosage of 10 mg/week, then based on 11.04% of the drug load, the theoretical GNPs/MTX-Cys-FA nanoconjugates that needs to be taken to the patient is 90.58 mg/week. However, nanoformulations still have some shortcomings, such as the need for multiple steps for preparation, a long synthesis cycle, and short storage time. This has brought difficulties to the formulation of

clinical applications and quality standards, thereby limiting the industrial production of nano-preparations. To break through the limitations of traditional preparation methods, microfluidic technology has received attention in the application of nano preparations. [17] In addition, it is also feasible to use 3D printed microfluidic devices to continuously synthesize nanoformulations. It is simple in design, quick to synthesize, and also has the advantages of low cost. These methods provide the possibility for the industrial production of nano-formulations. To investigate the safety of intravenously administered nanoparticles, a hemolysis experiment was performed. The hemolysis test is used to evaluate the biocompatibility of nanomedicines. Fig. 3 shows that when concentrations of GNPs (E), free MTX (F), and GNPs/MTXCys-FA (G) increased from 7.8 μ g/mL to 1000 μ g/mL, there was no obvious hemolysis (1%). Therefore, intravenous administrations of GNPs, free MTX, and GNPs/MTX-Cys-FA have good biocompatibilities. [18]

3.3. *In vitro* drug release behaviors of GNPs/MTX-Cys-FA

The HPLC method was used to evaluate *in vitro* release behaviors of MTX from nanoparticles. Fig. 2F shows that in both release media, GNPs/MTX-Cys-FA were released in two phases. Within 1 h, percentages of GNPs/MTX-Cys-FA released in PBS at pH 7.4 and pH 5.5 were 32% and 58%, respectively. This may be due



to dissolution of Cys near the nanoparticle surface in the release medium. At the same time, GNPs/ MTX-Cys-FA had acid-sensitive FA, which was rapidly degraded under acidic conditions, so that, GNPs/MTX-Cys-FA has a greater burst release at pH 5.5 PBS. Within 8 h, the release of GNPs/MTX-Cys-FA reached a plateau. At pH 7.4 PBS, about 59% of the drug was released, while 76% of the drug was released at pH 5.5 PBS, confirming that GNPs/MTX-CysFA exhibits acid-responsive characteristics. HPLC analysis showed that drug loading capacity of GNPs/MTX-Cys-FA was $11.04 \pm 0.28\%$, while its encapsulation efficiency was $73.61 \pm 1.91\%$. This is slightly different from drug loading in the TGA, which may be due to the fact that MTX was not completely dissolved when the supernatant was taken for the measurement of drug loading. Compared to high release values in this study, some studies reported relatively low release values. Tahari *et al.* (2011) found that total drug release in PBS solution within 3 days was only 3% and 5%. Jang *et al.* (2019) documented that the release rate of PLGA NPs

loaded with MTX was faster at low pH than at high pH. Within 48 h, drug release exceeded 80%, then, it gradually increased. These findings were comparable to ours.

3.4. In vitro cytotoxicity and cellular uptake of RAW264.7

The CCK-8 assay was performed to evaluate the cytotoxic effects of GNPs and GNPs/MTX-Cys-FA in LPS activated or non-activated RAW264.7 cells. These effects were compared to those of free MTX solutions (Fig. 4A and B). At $0.1 \mu\text{g/mL}$ – $50 \mu\text{g/mL}$, GNPs did not exhibit inhibitory effects on the viability of the cell line. These findings were consistent with those reported by James *et al.* (2015) who found that when macrophages were treated with GNPs in the concentration range of 0.1 – $60 \mu\text{M}$ for 24 h, cell viability was only slightly reduced. These findings prove that GNPs, as drug carrier materials, are nontoxic and have good biocompatibilities.

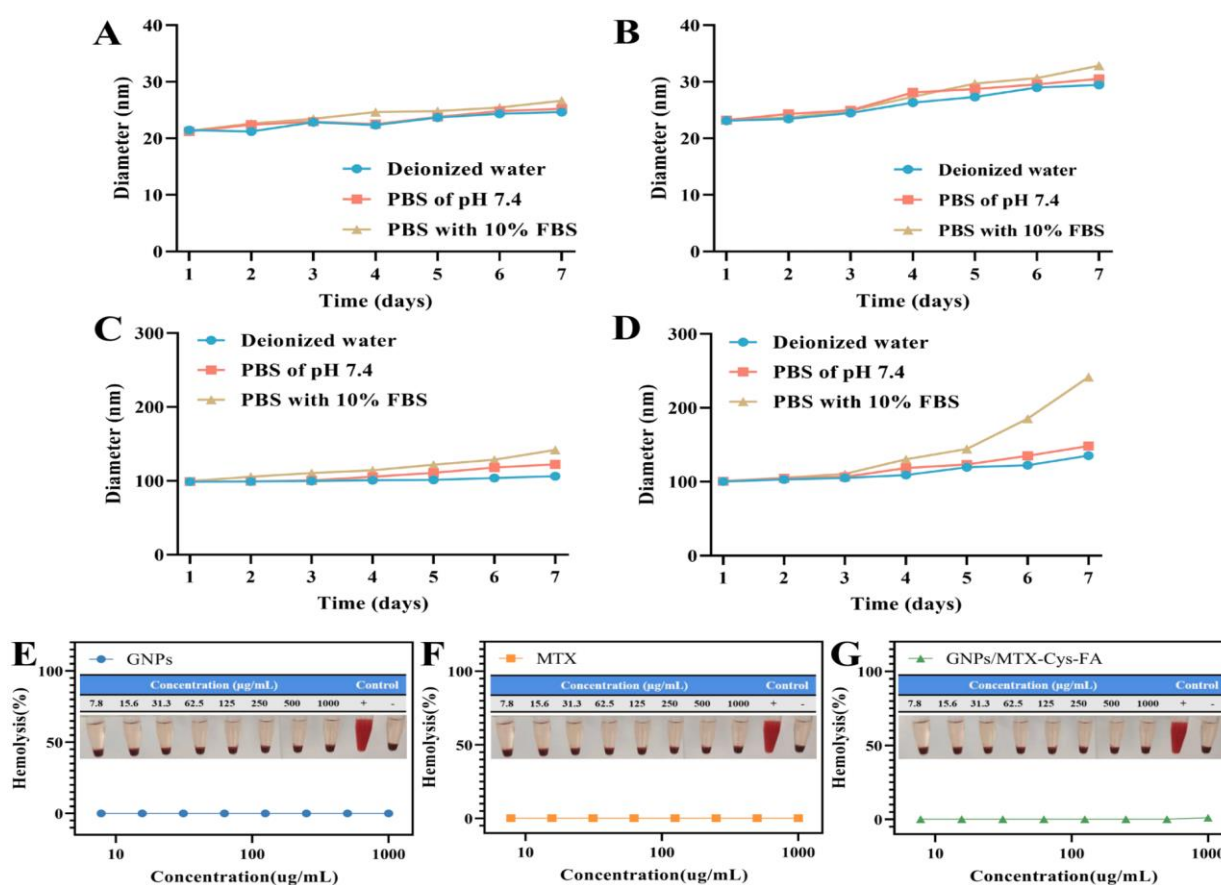


Fig.5. The colloidal stability of GNPs and GNPs/MTX-Cys-FA in different media ($n = 3$). (A and C) the particle size of GNPs in 4°C or 37°C , respectively. (B and D) particle size of GNPs/MTX-Cys-FA in 4°C or 37°C , respectively. Hemolysis behavior of different formulations of nanoconjugates on blood cells ($n = 6$). (E) blank GNPs, (F) free MTX, (G) GNPs/MTX-Cys-FA treated erythrocyte supernatant.



In addition, with decreasing MTX concentrations, cytotoxic effects were significantly reduced. An increase in concentrations of MTX and MTX-Cys-FA, freely existing or loaded in GNPs, enhanced the cytotoxicity. When concentrations of MTX and MTX-Cys-FA were maintained at 10 $\mu\text{g}/\text{mL}$, almost 80% of the cells were killed (Fig. 4C). Compared to GNPs/MTX-Cys-FA, free MTX exhibited a stronger toxic effect on the cell line. Through the nano-carrier system, the toxicity of MTX to healthy cells was reduced, proving that GNPs/MTX-Cys-FA can be used as a nano-drug carrier system to deliver MTX to the RA target site. These

findings is in tandem with those of previous studies. [19] To prove the *in-vitro* targeting abilities of GNPs/MTX-Cys-FA, we investigated the uptake of FITC-labeled GNPs/MTX-Cys-FA and GNPs/MTX-Cys by LPS activated and inactivated RAW264.7 cells. As shown in Fig. 4D, compared to GNPs/MTX-Cys-FITC, LPS activated cells significantly sequestered GNPs/MTX-Cys-FA-FITC. However, there were no significant differences in uptakes of GNPs/MTX-Cys-FA-FITC and GNPs/MTX-Cys-FITC by inactivated cells. We found that LPS activation enhanced the expression of FRs on surfaces of RAW264.7 cells, thereby enhancing FR-mediated GNPs/MTX-Cys-FA-FITC cell internalization, ultimately leading to a higher fluorescence intensity. To confirm the targeting of

GNPs/MTX-Cys-FA-FITC and GNPs/MTX-Cys-FITC to activated macrophages, flow cytometry was performed. Fig. 4E shows that, among all groups, the fluorescence intensity of GNPs/MTX-Cys-FA-FITC in LPS-activated RAW264.7 cells were the highest. In addition, fluorescence intensities of GNPs/MTX-Cys-FITC in LPS-activated RAW264.7 cells were close to fluorescence intensities of GNPs/MTX-Cys-FA-FITC and GNPs/MTX-Cys-FITC in non-activated cells. These findings imply that absorptions of FA-modified nanoparticles in cells is correlated with the presence of FR, consistent with cytotoxicity results. In conclusion, these findings imply that FA-targeted nanoparticles can effectively achieve targeting functions.

3.5. In vitro cytotoxicity, proliferation, horizontal migration assays

The CCK-8 assay was used to assess the cytotoxic effects of GNPs and GNPs/MTX-Cys-FA on HFLS-RA cells. At concentrations of 0.1–50 $\mu\text{g}/\text{mL}$, cell survival rate was greater than 80%, consistent with experimental results of RAW264.7 cells (Fig. 5A). In addition, concentrations of GNPs/MTX-Cys-FA were screened for cytotoxicity. Concentrations of 1.25 $\mu\text{g}/\text{mL}$, 2.5 $\mu\text{g}/\text{mL}$, and 5 $\mu\text{g}/\text{mL}$ which had cell viabilities of above The CCK-8 assay was used to determine cell proliferation levels in the GNPs/MTX-Cys-FA and free MTX treated groups (Fig. 5C).

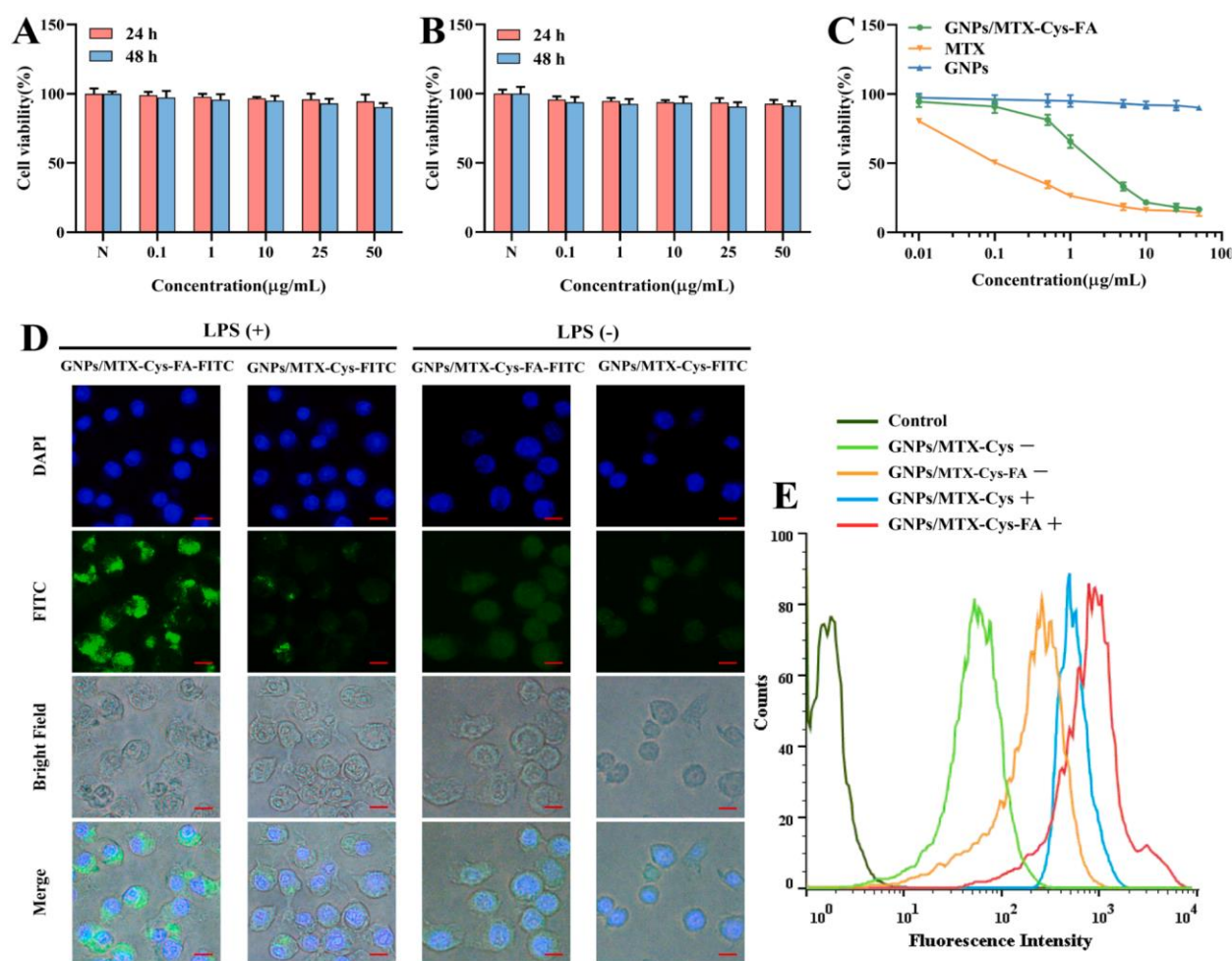


Fig. 6. Cytotoxicity and cellular uptake of RAW264.7. (A) The cytotoxicity of GNPs to inactivated RAW264.7. (B) The cytotoxicity of GNPs to the activation of RAW264.7. (C) The cytotoxicity of GNPs, MTX or GNP/MTX-Cys-FA to the activation of RAW264.7 within 24 h. The value is the mean \pm SD ($n = 6$). CLSM images (D) and FCM results (E) of RAW264.7 cells incubated with GNP/MTX-Cys-FA-FITC or GNP/MTX-Cys-FITC for 12 h. Scale: 10.0 μm . 80% were treated as low-dose, medium-dose, and high-dose groups, while a free MTX concentration of 2.5 $\mu\text{g/mL}$ was used as the positive control (Fig. 5B).

The TNF- α group exhibited the most significant improvement in HFLS-RA cells viability. Low GNP/MTX-Cys-FA concentrations (1.25 $\mu\text{g/mL}$) significantly increased cell proliferations. At high concentrations (5 $\mu\text{g/mL}$), cell viabilities were significantly suppressed, cell proliferation capacities were inhibited, and were time- as well as dose-dependent. Through their tumor-like migration and invasive properties, HFLSRA cells are involved in inflammation, affect cartilage degradation and the subsequent bone destruction. Therefore, it is important to use HFLS-RA as a DMARD targeted therapy for RA. To investigate the effects of GNP/MTX-Cys-FA and free MTX on horizontal and vertical migration abilities, HFLS-RA cells were induced by TNF- α , and treated with different concentrations of GNP/MTX-Cys-FA and free MTX at different time points. Fig. 5

shows that in TNF- α stimulated and non-stimulated cells, GNP/MTX-Cys-FA inhibited the migration of original HFLS-RA cells in a dose-dependent manner. These findings confirm that GNP/MTX-Cys-FA exerts time- and dose-dependent effects on horizontal (D and E) and vertical migration (F and G) of HFLS-RA. Compared to MTX (2.5 $\mu\text{g/mL}$), GNP/MTX-Cys-FA (2.5 $\mu\text{g/mL}$) exhibited a stronger inhibitory effect on horizontal and vertical migration. Inhibitory effects of GNP/MTX-Cys-FA (5 $\mu\text{g/mL}$) on horizontal and vertical migration of HFLS-RA cells were significantly stronger than those of MTX alone (2.5 $\mu\text{g/mL}$). These results show that GNP/MTX-Cys-FA can be used to deliver a lower dose of MTX, while achieving the same therapeutic effect and safer.

3.6. Pharmacokinetics and in vivo biodistribution



The plasma concentration-time curve of MTX after intravenous administration of free MTX and GNPs/MTX-Cys-FA nanoconjugate (equivalent dose of 1.5 mg/kg MTX) in male Wistar rats is shown in Fig. 6A. Plasma concentrations of free MTX were found to have dropped within 12 h after intravenous injection and were almost undetectable after 12 h. In the nanoconjugate group, MTX was capable of being detected at 24 h. Therefore, compared to the control group (free MTX), the nanoconjugate significantly reduced the plasma clearance rates of MTX ($p < 0.05$). Table 3 shows the pharmacokinetic parameters of the

two groups. The half-life ($t_{1/2}$) of the nanoconjugate was prolonged by a factor of 2.1 while the average residence time (MRT_0-t) was increased by a factor of 1.74 ($p < 0.01$), leading to increased MTX accumulation in inflamed joints. The C_{max} of the nanoconjugate increased by a factor of 1.1 while the V_{dss} increased by a factor of 1.04, proving that the degree of absorption and binding of the nanoconjugate to MTX was greater than that of free MTX. The area under the concentration-time curve (AUC_0-t), the main indicator of drug efficacy, was increased by factor of 2.0, thereby changing drug bioavailability.

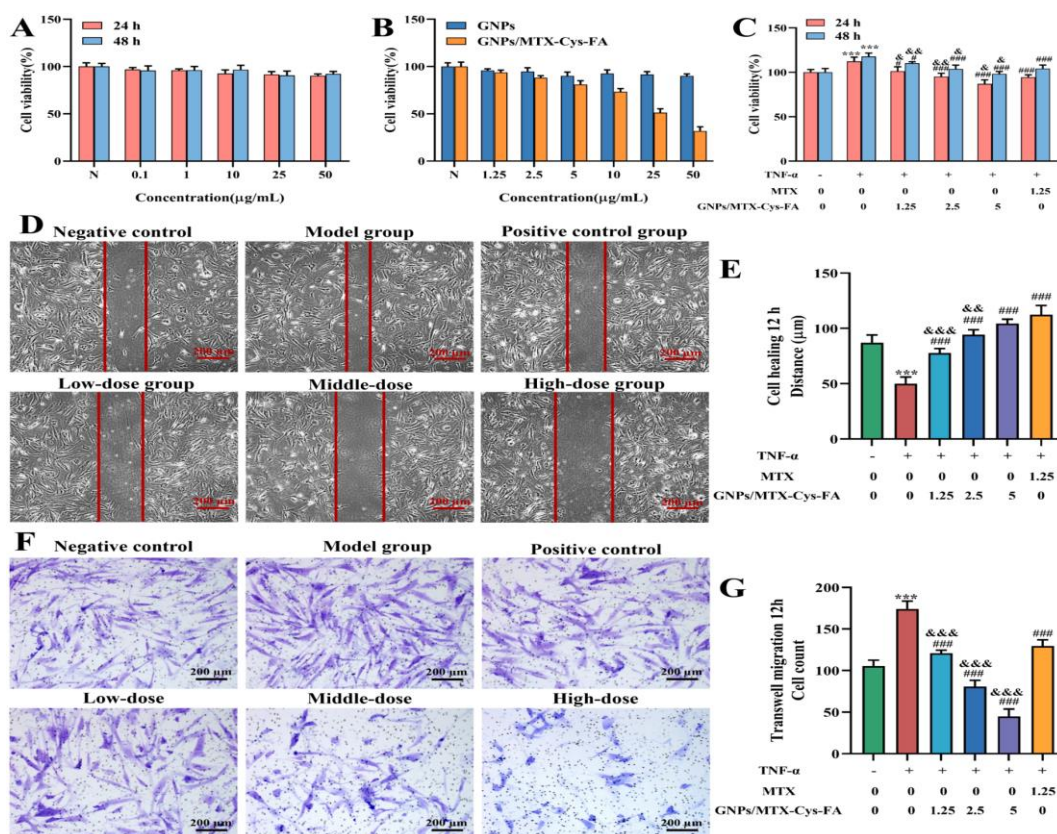


Fig.7. Cytotoxicity, cell proliferation, cell scratching and transwell test of HFLS-RA. (A) The toxicity of different concentrations of GNPs to HFLS-RA cells. (B) Toxicity of different concentrations of GNPs and GNPs/MTX-Cys-FA to HFLS-RA cells. (C) Cell proliferation induced by TNF- α at different concentrations of MTX and GNPs/MTX-Cys-FA. (D) The ability of HFLS-RA to migrate horizontally. (E) ImageJ measures the distance of horizontal migration of cells. (F) The ability of HFLS-RA to migrate vertically. (G) ImageJ measures the vertical migration distance of cells. * $P < 0.05$, ** $P < 0.01$ and *** $P < 0.001$, vs. Negative Control; # $P < 0.05$, ## $P < 0.01$ and ### $P < 0.001$ vs. TNF- α ; & $P < 0.05$ and && $P < 0.01$, vs. MTX.

MTX concentrations in different CIA rat model tissues were quantitatively measured by LC-MS/MS to evaluate *in vivo* biodistributions of free MTX and GNPs/MTX-Cys-FA nanoconjugates after intravenous administration. Fig. 6B and C shows that compared to free MTX, nanoconjugates inhibited MTX accumulation in the liver and spleen, indicating that they can effectively suppress MTX uptake by these

organs. In addition, after free MTX administration, MTX accumulation levels in the kidneys were increased, which may account for MTX-associated nephrotoxicity. [20] In contrast, the nanoconjugate administered group had lower amounts of MTX in the kidneys. Moreover, free MTX accumulation in inflamed joints of the nanocomposite were higher than those of the free MTX solution. We compared targeting



efficiencies by calculating the ratios of plasma concentrations of GNPs/MTX-Cys-FA in inflammatory joints to plasma concentrations of free MTX. The AUC_{0-24} of GNPs/MTX-Cys-FA was 6.9 times higher than that of free MTX. Compared to free MTX, accumulation of MTX from the GNPs/MTX-Cys-FA nanoconjugates reached its maximum at 2 h after administration. These findings prove that through GNPs and FA coupling, the EPR effect and active targeting ability of the nanoconjugate enhanced its accumulation in joints. We used the *in vivo* fluorescence imaging method to qualitatively observe and compare the distribution of free MTX, GNPs/MTX-Cys, and GNPs/MTX-Cys-FA nanoconjugates in joints (Fig. 6D). Our findings were consistent with our postulates. The GNPs/MTX-Cys-FA nanoconjugates were found to had the highest fluorescence intensity at each time point, consistent with *in vivo* tissue distribution outcomes. Compared to

free MTX, fluorescence signals in the bladder of CIA rats were significantly increased after administration of the GNPs/MTX-Cys nanoconjugates, indicating that it was metabolized by the kidney within 4 h. However, 2 h after administration of the GNPs/MTX-Cys-FA nanoconjugates, fluorescence signals in arthritic joints of CIA rats were significantly increased. Through quantitative analyses of optical densities, we found that high accumulation levels of GNPs/MTX-Cys-FA nanoconjugates in inflammatory joints of CIA rat models may be attributed to folate receptor-mediated endocytosis and rapid intracellular drug release. The GNPs/MTX-Cys-FA nanoconjugates last longer in circulation and selectively accumulate in arthritic joints. FA enhances the targeting ability of nanoconjugates and promotes their retention in arthritic joints, consistent with tissue biodistribution test results (Fig. 6E).

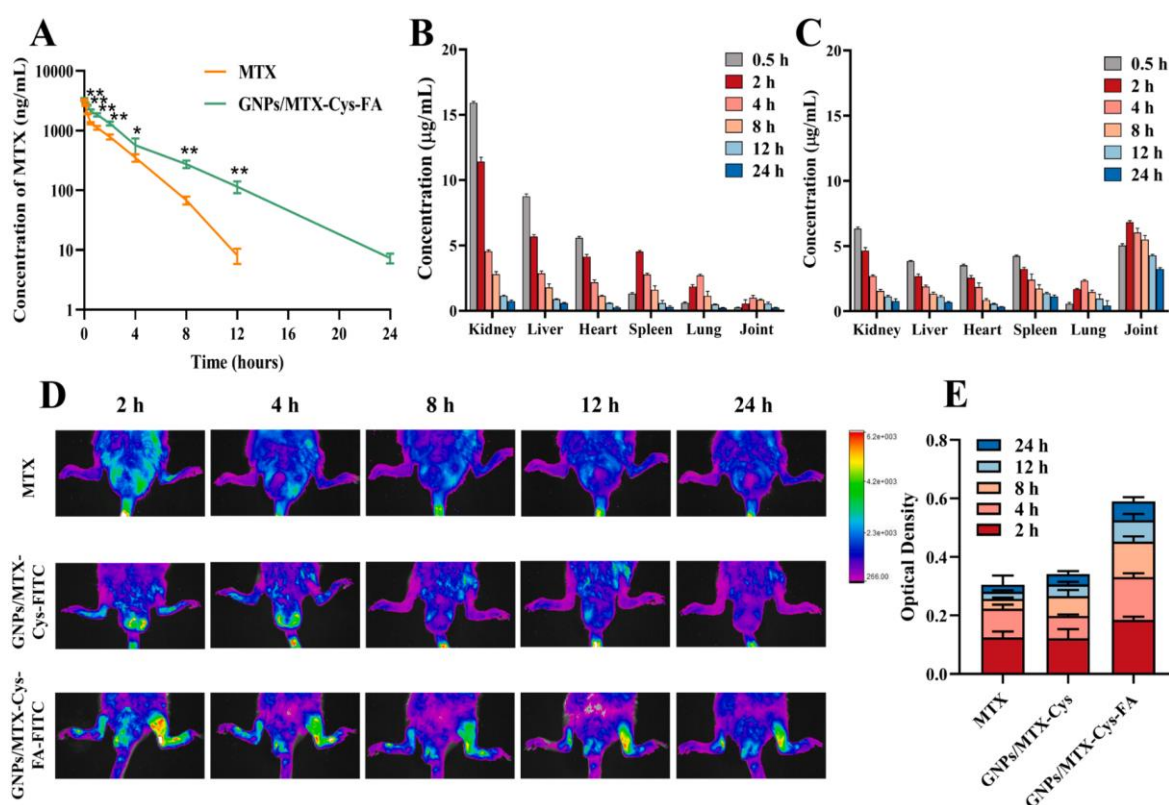


Fig. 8. Pharmacokinetics and distribution in rats. (A) The concentration versus time curve of MTX after intravenous injection of MTX and GNPs/MTX-Cys-FA in Wistar rats. MTX content in the heart, liver, spleen, lung, kidney and joints of CIA rats after intravenous injection of MTX (B) and GNPs/MTX-Cys-FA (C). (D) *In vivo* fluorescence imaging of CIA rats collected images in the range of excitation wavelength of 480 nm and emission wavelength of 530 nm. (E) ImageJ to quantify the fluorescence intensity of the optical density. Data represented as Mean \pm SD ($n = 6$). ** $P < 0.01$, * $P < 0.05$ vs. MTX solution.

Many studies have evaluated drug targeting functions from an *in vitro* fluorescence imaging perspective. Liu *et al.* (2019) established a CIA mouse arthritis model

and injected chlorine e6 labeled MTXHSA NMs. Fluorescence/magnetic resonance dual-mode imaging revealed that MTXHSA NMs was highly accumulated



and had a longer retention time in inflamed joints than free MTX molecules. Wang *et al.* (2019) used real-time fluorescence imaging to check the distribution of DiD fluorescently-labeled drugs in SD rat models. They found that RGD enhanced the targeting ability of micelles and promoted their retention in arthritic joints. In summary, the GNPs/MTX-Cys-FA nanoconjugate is a formula that can significantly improve MTX treatment of RA. At the same drug dose, side effects due to free MTX were significantly greater, implying that MTX delivery through nanoconjugates can significantly increase the efficacy of treating RA and significantly inhibit its toxic and side effects on the liver and kidney.

3.7. Therapeutic efficacy and expression of pro-inflammatory cytokines

The efficacy of new drugs in animal models is the most common evaluation index. The CIA rat model is the most widely used model for studying the pathogenesis of autoimmune arthritis and testing new

antiinflammatory and immunospecific therapies. [21] The arthritis index scores were used to evaluate the success of establishing the CIA rat models. As shown in Fig. 7A, the sum of arthritis indices of extremities of rats after 14 days of immunization was greater than 6 points, indicating that all rats had been successfully modeled. Then, CIA rats were intravenously administered with MTX and GNPs/MTX-Cys-FA through the tail vein, after every two days. To objectively evaluate the therapeutic effects in each group, toe volumes of rats were used to evaluate anti-inflammatory effects of free MTX and GNPs/MTX-Cys-FA. Fig. 7B shows that compared to the positive control group, after intravenous GNPs/MTX-Cys-FA injection, toe volumes of CIA rat models were significantly reduced while the degree of joint swelling was significantly improved. In addition, toe volumes of CIA rat models in the Blank group; & $P < 0.05$ and && $P < 0.01$, vs. Positive control group high-dose group were significantly reduced after GNPs/MTX-Cys-FA treatment. [22]

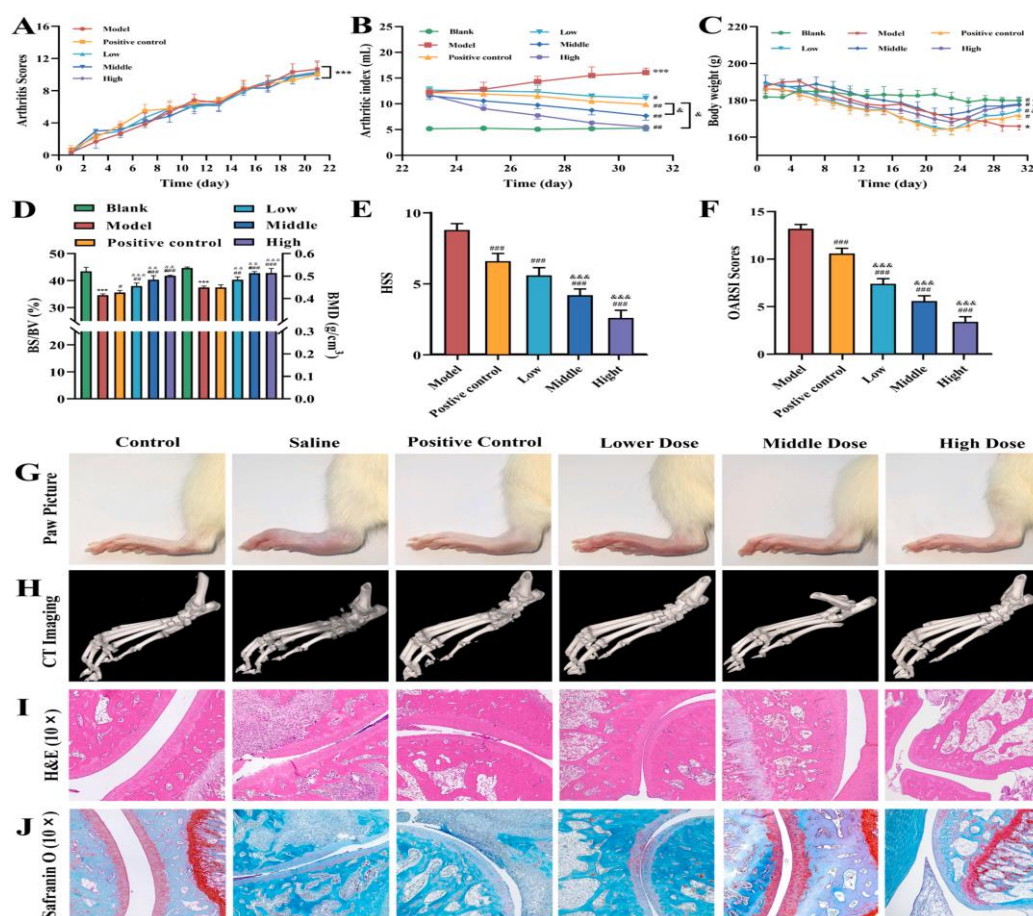


Fig.9. Evaluation of the therapeutic efficacy of free MTX and GNPs/MTX-Cys-FA. (A) The arthritis score of rats in each group. (B) Toe volume of rats in each group. (C) Body weight of mice in each group. (D) BS/BV and BMD of each group were detected by Micro CT scan. (E) Histological synovitis score (HSS) and (F) modified OARSI scores of joint tissues extracted from different treatment groups. (G) Macroscopic images and (H) micro computed tomography



(CT) measurement of the feet of mice in the different treatment groups. (I) Histological analysis with H&E and (J) safranin O staining of joint tissues extracted from mice of different treatment groups, scale bar 50 μm . Data are represented as Mean S.D. ($n = 6$). * $P < 0.05$, ** $P < 0.01$ and *** $P < 0.001$, vs. Model group; # $P < 0.05$, ## $P < 0.01$ and ### $P < 0.001$ vs.

As shown in Fig. 7G, to intuitively illustrate that free MTX and GNPs/MTX-Cys-FA can inhibit the swelling of inflamed joints by varying degrees, the rats' left hind feet were photographed and observed after 5 treatments. Compared to free MTX, CIA rat models treated with GNPs/MTX-Cys-FA exhibited the most effective inflammatory inhibitory effects. RA is characterized by proliferative synovitis, causing cartilage and bone destruction, which may cause osteopenia around the joints, erosion of the subchondral bone of the articular margin, systemic osteoporosis, and increased the risk of fractures. [23, 24] Therefore, we used Micro-CT to scan the joints of CIA rat models after treatment. In clinical RA, CT is important in the diagnosis and evaluation of bone erosion. Fig. 7H shows that compared to the blank group, the joints of CIA rat models in the model group exhibited obvious cartilage destructions and bone erosions. Compared to partial reduction of bone erosion by injection of free MTX, after intravenous GNPs/MTX-Cys-FA administration, inflamed joints of rats in the middle and high dose groups exhibited slightly eroded bone structures. The low dose treated mice groups were found have restored bone structures with moderate erosion. Fig. 7D shows that, compared to free MTX injection, bone surface/ volume ratios (BS/BV) and bone mineral density (BMD) of CIA rat models intravenously administered with GNPs/MTX-Cys-FA were found to have significantly improved, consistent with results from the Micro-CT scan. Therefore, CIA rat models treated with GNPs/MTX-Cys-FA exhibited the best therapeutic effects. This could be attributed to the high passive and active targeting of GNPs/MTX-Cys-FA. Compared to rat models administered with GNPs/MTX-Cys-FA, arthritis inflammation in CIA rat models treated with free MTX was moderately suppressed. [25]

This is because; GNPs/MTX-Cys-FA only exhibits dual targeting effect. To confirm the therapeutic effects

of the conjugate, histopathology analyses were performed. Fig. 7I shows that joint surfaces of the blank group were smooth without joint fibrosis and inflammatory cell infiltration. The articular cartilage of rats in the model group were invaded by many pro-inflammatory cytokines and proteases, resulting in rough articular surfaces, fibrous hyperplasia, and a large number of inflammatory cells infiltrating the hyperplastic synovium on the articular surface and around the joint, which translated in the highest HSS ($\text{HSS} > 8.0$) (Fig. 7E). Although the free MTX and the low-dose treatment group were relieved, mild infiltrations of inflammatory cells and synovial hyperplasia were still observed. Histopathological images of the GNPs/MTX-Cys-FA group revealed small amounts of inflammatory cell infiltration and small amounts of synovial hyperplasia in affected joints. The articular cartilage surface was smooth and intact, without damage and with an obvious joint cavity, implying alleviated arthritis cartilage damage. Similar results were obtained by Safranin O staining (Fig. 7J), which stains the glycosaminoglycans in the cartilage. An obvious proteoglycan loss was found in the model group, indicating serious degradation and damage of the articular cartilage. The cartilage appeared intact in the rats treated with GNPs/MTX-Cys-FA, which resulted in an OARSI histological score 2–3 folds lower than that of rats injected with an equivalent dose of free MTX (Fig. 7F). This findings are consistent with those of *in vitro* cell experiments. The middle dose and the high dose treated groups exhibited effectively inhibited synovial inflammations and protection of articular cartilage erosion. This was attributed to active targeting of FR and selective biodistribution in affected joints. In the active RA stage, pro-inflammatory cytokine levels are. These inflammatory cytokines activate osteoclasts and cause bone destructions. Therefore, serum pro-inflammatory cytokine levels are important markers for anti-arthritis drug efficacy. [26, 27]

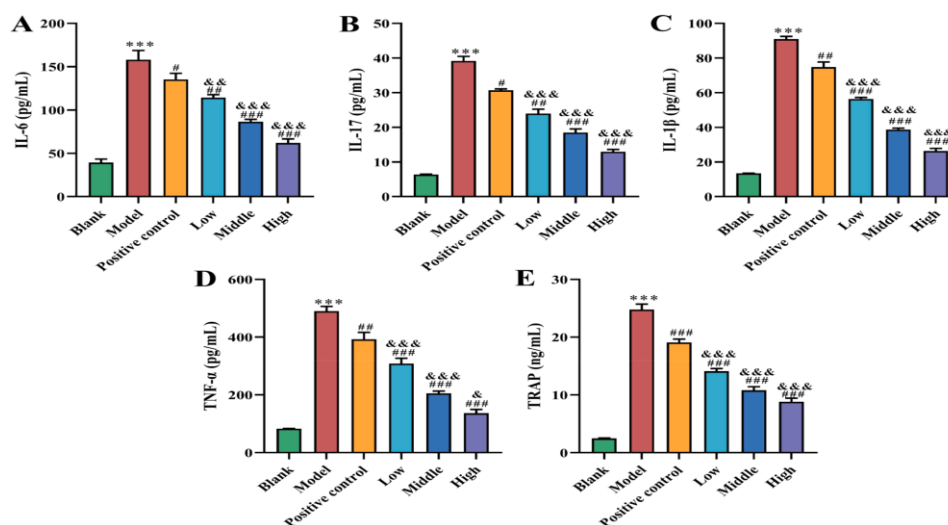


Fig.10. The levels of (A) IL-6, (B) IL-17, (C) IL-1 β , (D) TNF- α and (E) TRAP in the serum of rats in each group. * $P < 0.05$, ** $P < 0.01$ and *** $P < 0.001$, vs. Model group; # $P < 0.05$, ## $P < 0.01$ and ### $P < 0.001$ vs. Blank group; & $P < 0.05$ and && $P < 0.01$, vs. Positive control group. important markers for disease severity. Inflamed synoviums secrete many inflammatory cytokines, including TNF- α , IL-1 β , IL-6, and IL-17 among others.

TNF- α activates synovial macrophages, thereby inducing the secretion of other pro-inflammatory cytokines. [28] IL-1 β and TNF- α are secreted and produced by macrophages. They are important inflammatory mediators that can activate vascular endothelial cells to enable inflammatory infiltrations of joint synovium further aggravating inflammatory response. [29] IL-6 and IL-17 have the closest relationships with RA. IL-6 can promote immunoglobulin formation by B cells, induce the production of various cytokines, promote the release of rheumatoid factor, and promote inflammatory responses as well as tissue damage in RA patients. [30] IL-17 has a powerful pro-inflammatory effect. It can stimulate fibroblasts to secrete inflammatory factors, promote hematopoietic factor production, and cause vascular proliferation. Moreover, it can directly act on osteoclasts, stimulate osteoclast activation, and cause bone destruction. [31, 32] Osteoclasts play a key role in the destruction of RA bones. Tartrate resistant acid phosphatase (TRAP) is a landmark phosphatase for osteoclasts, and its activity can be used as an important marker for evaluating the activity of osteoclasts and bone resorption. [33, 34] Therefore, to investigate the effects of free MTX and GNP/MTX-Cys-FA on serum pro-inflammatory cytokine and osteoclast levels, we evaluated IL-6 (A), IL-17 (B), IL-1 β (C), TNF- α (D) in rat serum and TRAP (E) concentration changes. Fig. 8 shows that concentrations of pro-inflammatory cytokines increased significantly after saline treatment, reflecting inflammatory severity in CIA rat models, compared with the positive control group, GNP/MTX-Cys-FA can significantly reduce the concentration of IL-6, IL-17, IL-1 β , TNF- α and TRAP ($p < 0.01$). At the same time, osteoclast levels were found to be

significantly reduced ($p < 0.01$). In addition, inflammatory factor and osteoclast levels in the GNP/MTX-Cys-FA low-dose group and GNP/MTX-Cys-FA medium-dose group were significantly suppressed than those of the positive control group ($p < 0.01$). [35] This is because, GNP/MTX-Cys-FA has a high affinity for FRs that are overexpressed on activated macrophages in synovial hyperplasia. Costa Lima *et al.* (2015) developed a new type of invisible polymer nanospheres that can carry anti-inflammatory drugs and imaging agents by combining MTX and GNPs. They detected IL-1 β , IL-6, and TNF- α levels in serum. TNF- α levels were found to be significantly reduced, consistent with results from this study. MTX-loaded nanoparticles have also been reported in other studies. Thomas *et al.* (2011) used FA targeting nanoparticles to perform *in vitro* studies using macrophages and *in vivo* studies using collagen-induced arthritis rat models. They found that the nanoparticles reduced inflammatory arthritis parameters, including cartilage damage, ankle swelling, paw volume, and bone resorption. [36, 37] developed MTX and minocycline-loaded nanoparticles (MMNPs) to relieve inflammation and joint stiffness. *In vivo*, they found that intravenous MMNPs administration effectively suppressed arthritis. Based on the above results, the designed conjugate, namely GNP/MTX-Cys-FA, significantly inhibited synovitis in affected joints as well as the production of pro-inflammatory cytokines, thereby protecting the articular cartilage and preventing bone erosion and destruction. To evaluate the safety of nanoparticles, body weight changes of arthritic rat models were investigated after administration. Fig. 7C shows that RA enhanced joint pain, swelling, and stiffness of rat models, making



them unable to walk. Therefore, rat weights were slightly decreased during the modeling process. During treatment, body weights of rats in the MTX and GNPs/MTX-Cys-FA treatment groups continued to increase from day 23 to day 33. The weights of untreated healthy mice did not change significantly, indicating that GNPs/MTX-Cys-FA is safe. [38]

4. Conclusions

We successfully synthesized a nanoconjugate with FR targeting abilities and GNPs as a carrier, namely GNPs/MTX-Cys-FA. They exhibited suitable particle sizes, good stabilities, and excellent drug-carrying capacities. The nanoconjugates were approximately 103.6 nm in size and were stable at a pH of 7.4, which is suitable for selective passive accumulation in inflammatory joints through the EPR effect. In addition, FA, as a targeting molecule, was combined with GNPs/MTX-Cys for targeted drug delivery. *In vitro*, compared to free MTX, the nanoconjugate exhibited a higher cytotoxicity on LPS-activated RAW264.7 cells, and cellular uptake was significantly improved through FA-mediated endocytosis. Compared to free MTX, GNPs/MTX-Cys-FA exhibited good inhibitory abilities on migration of HFLS-RA cells. In addition, compared to free MTX, *in vivo* pharmacokinetic behaviors of the nanoconjugate were enhanced. Accumulation levels of GNPs/MTX-Cys-FA in inflamed joints were elevated while their therapeutic effects were enhanced. Importantly, GNPs/MTX-Cys-FA exhibited the least toxic effects to major organs. As described, GNPs/MTX-Cys-FA can significantly inhibit rheumatoid synovitis and effectively protect articular cartilage by inhibiting the expression and secretion of inflammatory factors. Therefore, GNPs/MTX-Cys-FA are promising drug delivery systems for targeted RA treatment.

Declaration of competing interest

The author declares no conflict of interest, financial or otherwise.

Acknowledgements

This research did not receive any specific grant from funding agencies in the public, commercial, or not-for-profit sectors. The authors are grateful to the National Institute of Technology (NIT), Rourkela, Odisha, India for providing all required facilities. The authors would also like to thank to Columbia Institute of Pharmacy, Raipur, Chhattisgarh, India for providing laboratory animal facilities.

References

1. Abbasi, M., Mousavi, M.J., Jamalzahi, S., Alimohammadi, R., Bezvan, M.H., Mohammadi, H., Aslani, S., 2019. Strategies toward rheumatoid

arthritis therapy; the old and the new. *J. Cell. Physiol.* 234 (7), 10018–10031.

2. Aletaha, D., Smolen, J.S., 2018. Diagnosis and Management of Rheumatoid Arthritis: a Review. *JAMA* 320 (13), 1360–1372.
3. Bandulasena, M.V., Vladisavljević, G.T., Odunmbaku, O.G., Benyahia, B., 2017. Continuous synthesis of PVP stabilized biocompatible gold nanoparticles with a controlled size using a 3D glass capillary microfluidic device. *Chem. Eng. Sci.* 171, 233–243.
4. Boisselier, E., Astruc, D., 2009. Gold nanoparticles in nanomedicine: preparations, imaging, diagnostics, therapies and toxicity. *Chem. Soc. Rev.* 38 (6), 1759–1782.
5. Chaabo, K., Kirkham, B., 2015. Rheumatoid Arthritis - Anti-TNF. *Int. Immunopharmacol.* 27 (2), 180–184.
6. Chandrupatla, D., Molthoff, C.F.M., Lammertsma, A.A., van der Laken, C.J., Jansen, G., 2019. The folate receptor β as a macrophage-mediated imaging and therapeutic target in rheumatoid arthritis. *Drug Deliv. Transl. Res.* 9 (1), 366–378.
7. Chen, M., Amerigos, J.C.K., Su, Z., Guissi, N.E.I., Xiao, Y., Zong, L., Ping, Q., 2019. Folate Receptor-Targeting and Reactive Oxygen Species-Responsive Liposomal Formulation of Methotrexate for Treatment of Rheumatoid Arthritis. *Pharmaceutics* 11 (11).
8. Cherkupally, P., Ramesh, S., de la Torre, B.G., Govender, T., Kruger, H.G., Albericio, F., 2014. Immobilized coupling reagents: synthesis of amides/peptides. *ACS Comb. Sci.* 16 (11), 579–601.
9. Devi, L., Gupta, R., Jain, S.K., Singh, S., Kesharwani, 2020. Synthesis, characterization and *in vitro* assessment of colloidal gold nanoparticles of Gemcitabine with natural polysaccharides for treatment of breast cancer. *J. Drug Deliv. Sci. Tec.* 56, 101565.
10. Fang, C., Shi, B., Pei, Y.Y., Hong, M.H., Wu, J., Chen, H.Z., 2006. *In vivo* tumor targeting of tumor necrosis factor- α -loaded stealth nanoparticles: effect of MePEG molecular weight and particle size. *Eur. J. Pharm. Sci.* 27 (1), 27–36.
11. Gong, T., Tan, T., Zhang, P., Li, H., Deng, C., Huang, Y., Gong, T., Zhang, Z., 2020. Palmitic acid-modified bovine serum albumin nanoparticles target scavenger receptor-A on activated macrophages to treat rheumatoid arthritis. *Biomaterials* 258, 120296.
12. Hao, F., Lee, R.J., Zhong, L., Dong, S., Yang, C., Teng, L., Meng, Q., Lu, J., Xie, J., Teng, L., 2019. Hybrid micelles containing methotrexate-conjugated polymer and co-loaded with microRNA-



- 124 for rheumatoid arthritis therapy. *Theranostics* 9 (18), 5282–5297.
13. Huang, C.C., Chiou, C.H., Liu, S.C., Hu, S.L., Su, C.M., Tsai, C.H., Tang, C.H., 2019. Melatonin attenuates TNF- α and IL-1 β expression in synovial fibroblasts and diminishes cartilage degradation: implications for the treatment of rheumatoid arthritis. *J. Pineal Res.* 66 (3), e12560.
14. Janakiraman, K., Krishnaswami, V., Sethuraman, V., Natesan, S., Rajendran, V., Kandasamy, R., 2019. Development of Methotrexate and Minocycline Loaded Nanoparticles for the Effective Treatment of Rheumatoid Arthritis. *AAPS PharmSciTech* 21 (2), 34.
15. Jang, J.H., Jeong, S.H., Lee, Y.B., 2019. Preparation and In Vitro/In Vivo Characterization of Polymeric Nanoparticles Containing Methotrexate to Improve Lymphatic Delivery. *Int. J. Mol. Sci.* 20 (13).
16. Jensen, K.J., 2013. Solid-phase peptide synthesis: an introduction. *Methods Mol. Biol.* 1047, 1–21.
17. Kesharwani D., Paliwal R., Satapathy T., Paul S. D., 2019. Rheumatoid Arthritis: An Updated Overview of Latest Therapy and Drug Delivery. *J Pharmacopuncture.* 22(4): 210–224. doi: 10.3831/KPI.2019.22.029
18. Kim, G.W., Lee, N.R., Pi, R.H., Lim, Y.S., Lee, Y.M., Lee, J.M., Jeong, H.S., Chung, S.H., 2015a. IL-6 inhibitors for treatment of rheumatoid arthritis: past, present, and future. *Arch. Pharm. Res.* 38 (5), 575–584.
19. Leamon, C.P., Reddy, J.A., Vlahov, I.R., Vetzal, M., Parker, N., Nicoson, J.S., Xu, L.C., Westrick, E., 2005. Synthesis and biological evaluation of EC72: a new folatetargeted chemotherapeutic. *Bioconjug. Chem.* 16 (4), 803–811.
20. Liu, L., Hu, F., Wang, H., Wu, X., Eltahan, A.S., Stanford, S., Bottini, N., Xiao, H., Bottini, M., Guo, W., Liang, X.J., 2019. Secreted Protein Acidic and Rich in Cysteine Mediated Biomimetic Delivery of Methotrexate by Albumin-Based Nanomedicines for Rheumatoid Arthritis Therapy. *ACS Nano* 13 (5), 5036–5048.
21. Ma, D.Q., Rajewski, R.A., Stella, V.J., 1999. New injectable melphalan formulations utilizing (SBE)(7m)- β -CD or HP- β -CD. *Int. J. Pharmaceut.* 189 (2), 227–234.
22. Mateen, S., Zafar, A., Moin, S., Khan, A.Q., Zubair, S., 2016. Understanding the role of cytokines in the pathogenesis of rheumatoid arthritis. *Clin. Chim. Acta* 455, 161–171.
23. Moghimi, S.M., Hunter, A.C., Murray, J.C., 2001. Long-circulating and target-specific nanoparticles: theory to practice. *Pharmacol. Rev.* 53 (2), 283–318.
24. Nguyen, H.T., Phung, C.D., Thapa, R.K., Pham, T.T., Tran, T.H., Jeong, J.H., Ku, S.K., Choi, H.G., Yong, C.S., Kim, J.O., 2018. Multifunctional nanoparticles as somatostatin receptor-targeting delivery system of polyaniline and methotrexate for combined chemo-photothermal therapy. *Acta Biomater.* 68, 154–167.
25. Oliveira, I.M., Gonçalves, C., Oliveira, E.P., Simon-Vazquez, R., da Silva Morais, A., Gonzalez-Fernandez, A., Reis, R.L., Oliveira, J.M., 2021. PAMAM dendrimers functionalised with an anti-TNF α antibody and chondroitin sulphate for treatment of rheumatoid arthritis. *Mater. Sci. Eng. C Mater. Biol. Appl.* 121, 111845.
- Onay Uçar, E., Sengelen, A., 2019. Resveratrol and siRNA in combination reduces Hsp27 expression and induces caspase-3 activity in human glioblastoma cells. *Cell Stress Chaperones* 24 (4), 763–775.
26. Pandolfi, F., Franza, L., Carusi, V., Altamura, S., Andriollo, G., Nucera, E., 2020. Interleukin-6 in Rheumatoid Arthritis. *Int. J. Mol. Sci.* 21 (15).
27. Radner, H., Aletaha, D., 2015. Anti-TNF in rheumatoid arthritis: an overview. *Wien. Med. Wochenschr.* 165 (1–2), 3–9.
28. Shea, B., Swinden, M.V., Tanjong Ghogomu, E., Ortiz, Z., Katchamart, W., Rader, T., Bombardier, C., Wells, G.A., Tugwell, P., 2013. Folic acid and folinic acid for reducing side effects in patients receiving methotrexate for rheumatoid arthritis. *Cochrane Database Syst. Rev.* 2013 (5), Cd000951.
29. Silman, A.J., Pearson, J.E., 2002. Epidemiology and genetics of rheumatoid arthritis. *Arthritis Res.* 4 (Suppl 3), S265–S272. Suppl 3. Sparks, J.A., 2019. Rheumatoid Arthritis. *Ann. Intern. Med.* 170 (1), Itc1–itc16.
30. Tateiwa, D., Yoshikawa, H., Kaito, T., 2019. Cartilage and Bone Destruction in Arthritis: pathogenesis and Treatment Strategy: a Literature Review. *Cells* 8 (8).
31. Thomas, T.P., Goonewardena, S.N., Majoros, I.J., Kotlyar, A., Cao, Z., Leroueil, P.R., Baker Jr., J.R., 2011. Folate-targeted nanoparticles show efficacy in the treatment of inflammatory arthritis. *Arthritis Rheum.* 63 (9), 2671–2680.
32. Udalova, I.A., Mantovani, A., Feldmann, M., 2016. Macrophage heterogeneity in the context of rheumatoid arthritis. *Nat. Rev. Rheumatol.* 12 (8), 472–485.
33. Van der Woude, D., van der Helm-van Mil, A.H.M., 2018. Update on the epidemiology, risk factors, and disease outcomes of rheumatoid arthritis. *Best Pract. Res. Clin. Rheumatol.* 32 (2), 174–187.
34. Wang, Y., Liu, Z., Li, T., Chen, L., Lyu, J., Li, C., Lin, Y., Hao, N., Zhou, M., Zhong, Z., 2019.



Enhanced Therapeutic Effect of RGD-Modified Polymeric Micelles Loaded With Low-Dose Methotrexate and Nimesulide on Rheumatoid Arthritis. *Theranostics* 9 (3), 708–720.

35. Widemann, B.C., Adamson, P.C., 2006. Understanding and managing methotrexate nephrotoxicity. *Oncologist* 11 (6), 694–703.
36. Xiao, S., Tang, Y., Lv, Z., Lin, Y., Chen, L., 2019. Nanomedicine - advantages for their use in rheumatoid arthritis theranostics. *J. Control. Release* 316, 302–316.
37. Yang, M., Feng, X., Ding, J., Chang, F., Chen, X., 2017. Nanotherapeutics relieve rheumatoid arthritis. *J. Control. Release* 252, 108–124.
38. Zhou, M., Hou, J., Zhong, Z., Hao, N., Lin, Y., Li, C., 2018. Targeted delivery of hyaluronic acid-coated solid lipid nanoparticles for rheumatoid arthritis therapy. *Drug Deliv.* 25 (1), 716–722.